Measurement of the angular correlations for the $^{16}O(e,e'n)^{15}O$ reaction in the giant resonance region

K. Kino, T. Saito,* Y. Suga,† and M. Oikawa‡
Laboratory of Nuclear Science, Tohoku University, Mikamine, Taihaku-ku, Sendai 982-0826, Japan

T. Nakagawa§ and T. Tohei§
Department of Physics, Tohoku University, Aramaki, Aoba-ku, Sendai 980-8578, Japan

K. Abe
Department of Engineering, Tohoku University, Aramaki, Aoba-ku, Sendai 980-8579, Japan

H. Ueno
Department of Physics, Yamagata University, Kojirakawa, Yamagata 990-8560, Japan
(Received 10 November 2000; published 15 January 2002)

Angular correlations have been measured for the $^{16}O(e,e'n_0)$ and $^{16}O(e,e'n_3)$ reactions in the energy region $\omega=20-31$ MeV at a momentum transfer of 0.33 fm^{-1}. They indicate dominance of the giant dipole resonance. The data are compared with a random-phase approximation calculation. A predicted backward-peaked angular correlation in the neutron decay, due to interference between the $T=0$ and $T=1$ resonances, was not observed. Legendre coefficients extracted from the angular correlation data suggest the existence of a broad $E2$ resonance over the giant dipole resonance region. The opposite signs of the correlation parameters b_1 and b_3 for the $^{16}O(e,e'n_0)$ and $^{16}O(e,e'p_0)$ reactions suggest that the $E2$ resonance below about 22 MeV is isoscalar. Above about 22 MeV, large positive values for b_1 and b_2 in $^{16}O(e,e'p_0)$ compared to small ones in $(e,e'n_0)$ reflect the contribution resulting from the direct-knockout process in $(e,e'p_0)$. The angular correlations for $^{16}O(e,e'n_3)$ and $^{12}C(e,e'n_0)$ were confirmed to be similar as expected from the similarity of their particle-hole configurations. The good agreement including the fine structure between the form factors for $^{16}O(e,e'n_0)$ and $^{16}O(\gamma,n_0)$ confirmed the dominance of the giant dipole resonance in this energy region.

DOI: 10.1103/PhysRevC.65.024604 PACS number(s): 25.30.Rw, 24.30.Cz, 23.20.En, 27.20.+n

I. INTRODUCTION

The giant dipole resonance (GDR) region of ^{16}O has been extensively studied. Much effort has been made to investigate multipole resonances other than dipole. This has been done using various probes. The isoscalar giant quadrupole resonance (IS-GQR) which has a centroid energy of about 21 MeV has been observed in the $^{16}O(\alpha,\alpha')$ [1,2], $^{16}O(\alpha,\alpha'\alpha)$ [3], and $^{16}O(e,e'\alpha)$ [4] reactions. On the other hand, $E2$ strength above the IS-GQR has also been observed in the $^{16}O(\gamma,n_0)$ [5] and $^{15}N(\vec{p},\gamma_0)^{16}O$ [6,7] reactions. However, these reactions are sensitive to both isoscalar and isovector (IV) excitations, so that it is possible that the IV-GQR strength might be present in the higher-energy region of the GDR. In reality there is still significant ambiguity as to the magnitude and distribution of the IV-GQR strength because of the low momentum transfer in experiments using real photons.

The $(e,e'p)$ and $(e,e'n)$ coincidence reactions might provide information on the IS-GQR and IV-GQR. Recently Cavinato *et al.* reported a random-phase approximation (RPA) calculation for the $^{16}O(e,e'x)$ reaction [8–10]. They showed that as a result of interference between the IV-GDR and IS-GQR, the angular correlations for the $(e,e'p_0)$ and $(e,e'n_0)$ reactions were quite different at $\omega=21$ MeV, while the correlations were similar at $\omega=30$ MeV because of interference between the same IV-GDR and IV-GQR. Thus information on the IV-GQR may be obtained from comparison of the $(e,e'p_0)$ and $(e,e'n_0)$ angular correlations. Although $(e,e'p)$ coincidence experiments have been extensively performed, there are only a few $(e,e'n)$ experiments [11–18] because of the experimental difficulties associated with the huge γ-ray background in electron scattering. The $^{16}O(e,e'p)^{15}O$ angular correlations have been measured by Dmitriev *et al.* at Novosibirsk [19] and by Zimmermann at Mainz [20], but no data for the $^{16}O(e,e'n)$ reaction are available. The present paper reports a measurement of the angular correlations for the $^{16}O(e,e'n_0)$ and $^{16}O(e,e'n_3)$ reactions in the giant resonance region and compares the results with those of the $^{16}O(e,e'p_0)$ and $^{16}O(\gamma,n)$ reactions and the RPA predictions.

II. EXPERIMENTAL PROCEDURE

The experiment was performed using the 129-MeV continuous electron beam from the 150-MeV Tohoku University pulse stretcher ring [21]. The duty factor and beam current

*Present address: Faculty of Engineering, Tohoku Gakuin University, Chuo, Tagajo 985-8537, Japan.
†Present address: Hitachi Software Engineering Co., Nakase, Mihama-ku, Chiba 261-0023, Japan.
‡Present address: 5th Research Center, Technical Research & Development Institute, Japan Defense Agency, Nagase, Yokosuka 239-0826, Japan.
§Present address: Tohoku Institute of Technology, Kasumicho, Taihaku-ku, Sendai 982-8577, Japan.

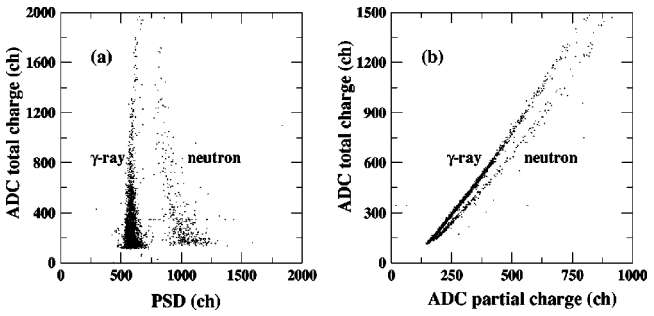

FIG. 1. n/γ discrimination by the (a) PSD module and (b) charge comparison method. The horizontal axis in (b) is the charge in the pulse tail.

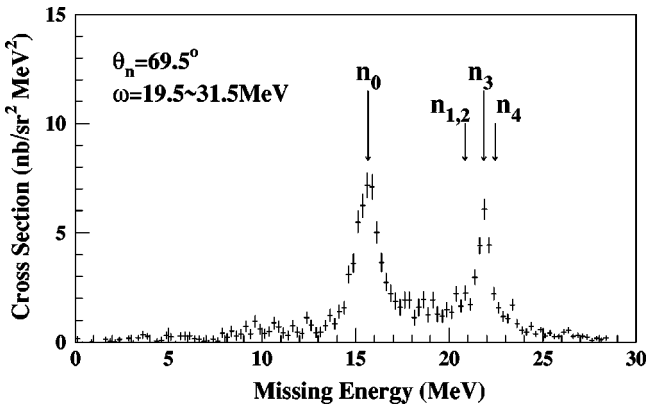

FIG. 2. Missing energy spectrum for the $^{16}O(e,e'n)^{15}O$ reaction at $\theta_n = 69.5°$. Arrows corresponding to the n_0, n_1, n_2, n_3, and n_4 transitions are indicated. The peaks for n_1, n_2, and n_4 were not seen obviously. Neutrons with lower energies than 2.5 MeV are excluded because of the low detection efficiency.

were ~80% and ~100 nA, respectively. A disk of 100.6 mg/cm^2 natural Li_2O (92.5% ^{7}Li and 99.8% ^{16}O) was used as the target. In order to take into account the contamination due to Li, several measurements using a natural Li target (90 mg/cm^2) were done under the same experimental conditions.

The scattered electrons were detected and momentum analyzed by a double-focusing magnetic spectrometer at a scattering angle of 30°. The spectrometer has a solid angle of 5 msr and a momentum resolution of 0.05% within an accepted momentum bite of 5.3%. After passing a magnetic field, electrons were detected by a vertical drift chamber (VDC) which was located on the focal plane to provide position and momentum information for each electron. Three layers of plastic scintillators of thicknesses 5, 5, and 8 mm located behind the VDC produced fast signals, and their coincident signals were used as a trigger for the electron arm.

Neutrons were detected using ten liquid-scintillation counters placed in the scattering plane around the target at the distance of 1.05 m. The angles of these detectors were 49.4°, 69.5°, 89.7°, 112.2°, 133.1°, 155.6°, 208.6°, 228.9°, 249.5°, and 269.8° to the beam direction. Each detector consisted of 2.54 *l* of NE213 and a 5-in. photomultiplier. The detectors were shielded from the huge γ-ray and neutron backgrounds by lead, paraffin, and concrete blocks. The scattered electrons and γ rays from the target were absorbed by 4- or 6-cm-thick ^{209}Bi plates, which were set in front of each detector. ^{209}Bi is a superior absorbing material because of its high attenuation for electrons and γ rays, and its low and energy-insensitive neutron-absorption coefficient. In order to remove γ-ray events we used pulse shape discriminator (PSD) modules and the charge comparison method. Figure 1 shows that they worked well. The neutron energy was determined from the time of flight (TOF) between the target and each neutron detector.

The detection threshold of the neutron detectors was chosen to be 3/4 of the pulse hight of the ^{137}Cs γ-ray Compton edge, which corresponds to a 1.27 MeV neutron. The neutron detection efficiency was obtained by a combination of two methods. The energy dependence of the efficiency near threshold was determined by measuring neutrons from a ^{252}Cf source. The relative efficiency as a function of the neutron energy in the higher-energy region and the absolute efficiency were calculated by a code TOTEFF [22]. The resulting efficiency increases from the threshold and reaches a maximum of 0.36 at about 3 MeV. It varies between 0.29 to 0.36 depending on the neutron energy, up to 15 MeV. A detailed description of the neutron efficiency is presented in Ref. [23].

III. RESULTS AND DATA ANALYSIS

A. Missing energy spectrum

The experiment was done in the excitation energy range from 20 to 31 MeV at a momentum transfer of 0.33 fm^{-1}. This covers the entire GDR region of ^{16}O. Figure 2 shows a typical missing energy spectrum for the $^{16}O(e,e'n)$ reaction. The contribution from Li was subtracted using the missing energy spectra obtained by the $^{NAT}Li(e,e'n)$ reaction taken under the same experimental conditions. There are two peaks at 15.7 and 21.8 MeV in the spectrum. The lower one corresponds to neutron decay to the ground state of the ^{15}O residual nucleus. The higher one is considered to correspond to neutron decay to the third excited state ($J^\pi = 3/2^-$), which is known to be a $1p_{3/2}$ neutron-hole state based on the ^{16}O ground state. The dominance of these two decay channels might imply that the giant resonances in light nuclei tend to decay directly from coherent one-particle–one-hole (1p-1h) excitations. No obvious peaks are seen that correspond to the first, second, or fourth excited states, which have positive parity. This feature is very similar to the situation for $^{16}O(e,e'p)$ experiment [19], which also shows the main decays to the ground and third excited states. The $^{16}O(\gamma,p\gamma')$ and $^{16}O(\gamma,n\gamma')$ reactions [24] also show dominant decay to the third excited state in each residual nucleus.

B. Angular correlations

1. Data analysis

The angular correlations for the $^{16}O(e,e'n_0)$ and $^{16}O(e,e'n_3)$ reactions are shown in Figs. 3 and 4, respectively. The data were fitted with Legendre polynomials as described below.

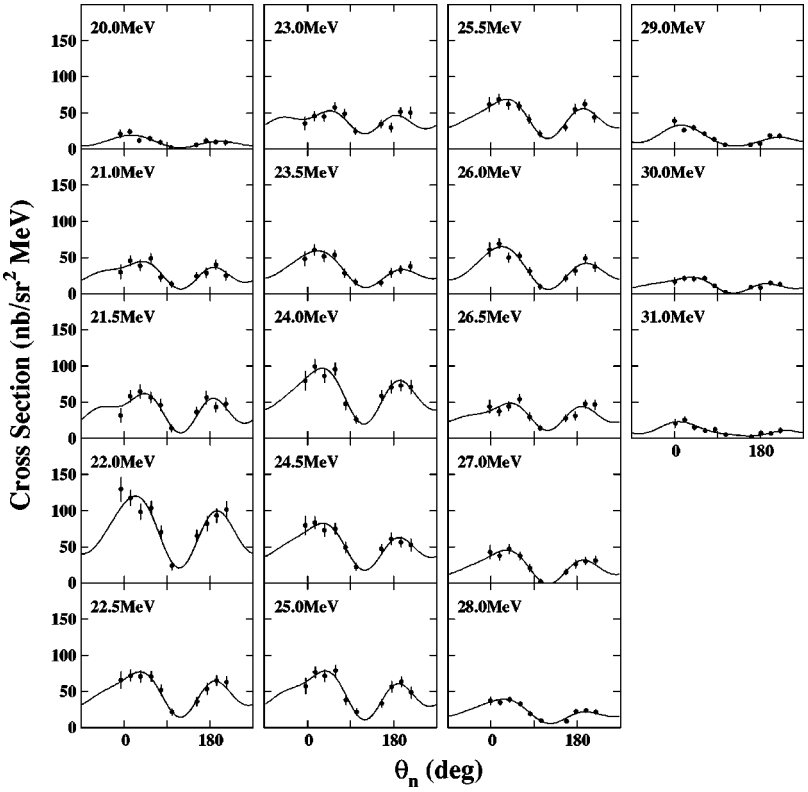

FIG. 3. Angular correlations for the $^{16}\mathrm{O}(e,e'n_0)$ reaction. The neutron angles are relative to the momentum transfer direction. The solid lines are χ^2 fits to the data by Legendre polynomials.

The $(e,e'x)$ reaction cross section is represented as follows [25]:

$$\frac{d^3\sigma}{d\omega\Omega_e\Omega_x} = \sigma_{\mathrm{Mott}}\{V_{\mathrm{L}}W_{\mathrm{L}} + V_{\mathrm{T}}W_{\mathrm{T}} + V_{\mathrm{LT}}W_{\mathrm{LT}}\cos(\phi) + V_{\mathrm{TT}}W_{\mathrm{TT}}\cos(2\phi)\}, \tag{3.1}$$

where "L" and "T" stand for the terms contributed by the longitudinal- and transverse-polarized virtual photons, respectively. The kinematical factors V_i are defined by the incident and scattered electrons, and W_i are the nuclear structure functions. The angle ϕ between the scattering and reaction planes has an effect on the interference terms $V_{\mathrm{LT}}W_{\mathrm{LT}}$ and $V_{\mathrm{TT}}W_{\mathrm{TT}}$, and is π in the present experiment.

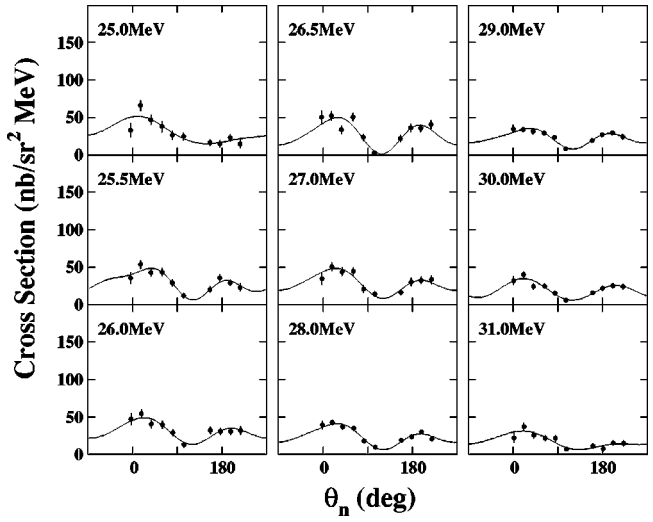

FIG. 4. Angular correlations for the $^{16}\mathrm{O}(e,e'n_3)$ reaction. The solid lines are the same as in Fig. 3.

First, we assumed that the main contribution to the cross section is $E1$, and the other excitations can be observed in the angular correlation through interference with $E1$. This $E1$ dominance has been studied experimentally by electron scattering measurements [26]. Each term $V_{\mathrm{L}}W_{\mathrm{L}}$, $V_{\mathrm{T}}W_{\mathrm{T}}$, $V_{\mathrm{LT}}W_{\mathrm{LT}}$, and $V_{\mathrm{TT}}W_{\mathrm{TT}}$ can be expanded assuming a maximum excitation multipolarity of 2 [27]:

$$V_{\mathrm{L}}W_{\mathrm{L}} + V_{\mathrm{T}}W_{\mathrm{T}} = \sum_{l=0}^{3} b_l P_l(x),$$

$$V_{\mathrm{LT}}W_{\mathrm{LT}} = \sum_{l=1}^{3} c_l P_l^1(x), \tag{3.2}$$

$$V_{\mathrm{TT}}W_{\mathrm{TT}} = \sum_{l=2}^{3} d_l P_l^2(x), \tag{3.3}$$

$$x = \cos(\theta_x). \tag{3.4}$$

Here, $P_l(x)$, $P_l^1(x)$, and $P_l^2(x)$ are Legendre polynomials and their associated functions, and b_l, c_l, and d_l are fit parameters which reflect the transition matrix elements. The ratio of the reduced matrix elements for transverse transitions to longitudinal ones is estimated from Siegert's theorem [28] to be 0.5 and 0.43 for $E1$ and $E2$, respectively. The kinematical factors V_{T} and V_{TT} are smaller than V_{L} or V_{LT} under the present experimental conditions, so that the ratios $V_{\mathrm{T}}W_{\mathrm{T}}/V_{\mathrm{L}}W_{\mathrm{L}}$ and $V_{\mathrm{TT}}W_{\mathrm{TT}}/V_{\mathrm{L}}W_{\mathrm{L}}$ become of the order of

0.1–0.2, and we ignored them. We also regarded c_1 and c_3 as terms small enough to be ignored, because they are $E1$-$E0$ or $E2$ interference terms in which at least one of the $E1$ or $E2$ transition is transverse. For W_{LT} the following relation between c_2 and b_2 results from Siegert's theorem [28] in the long-wavelength limit approximation for $E1$:

$$c_2 = -\frac{\omega}{q} b_2 . \tag{3.5}$$

Finally, including the kinematical factors V_i in the redefined parameters, we get the following representation for the angular correlation:

$$\frac{d^3\sigma}{d\omega\Omega_e\Omega_x} = A_0 \Bigg\{ 1 + b_1 P_1(x) + b_2 P_2(x) + b_3 P_3(x) + \frac{V_{\mathrm{LT}}}{V_{\mathrm{L}}} \frac{\omega}{q} b_2 P_2^1(x) \Bigg\},$$

$$x = \cos(\theta_x). \tag{3.6}$$

Here, $4\pi A_0$ represents the total cross section. The solid lines in Figs. 3 and 4 are the results of least-squares fits using the above equation.

2. $^{16}O(e,e'n_0)$ and $^{16}O(e,e'n_3)$ angular correlations

The angular correlations for the $^{16}\mathrm{O}(e,e'n_0)$ and $^{16}\mathrm{O}(e,e'n_3)$ reactions as shown in Figs. 3 and 4 have forward and backward peaks. This correlation indicates that the GDR is the main process and is reproduced by the $b_2P_2(x)$ term in Eq. (3.6). There is a small forward and backward asymmetry. This is due to interference between the GDR and other excitations with even parity. This asymmetry is reproduced by the $b_1P_1(x)$ and $b_3P_3(x)$ terms in Eq. (3.6). These peaks shift towards larger angles from the momentum transfer direction or antidirection, respectively. This is caused by interference between the strong longitudinal and weak transverse transitions, which is reproduced by the $(V_{\mathrm{LT}}/V_{\mathrm{L}})(\omega/q)b_2P_2^1(x)$ term in Eq. (3.6).

Figure 5 shows the fit parameters for the $^{16}\mathrm{O}(e,e'n_0)$ and $^{16}\mathrm{O}(e,e'n_3)$ angular correlations together with those for $^{16}\mathrm{O}(e,e'p_0)$. The n_0 form factor shown in Fig. 5(a) has two peaks at 22 and 24 MeV, which agrees with the typical structure of the ^{16}O GDR. The n_3 strength obtained above 25 MeV is similar to that of n_0. The parameter b_2 reflects the particle-hole configurations of the GDR. The $(s_{1/2},1p_{1/2}^{-1})$ and $(d_{3/2},1p_{1/2}^{-1})$ configurations are assigned for the n_0 transition. The observed b_2 value $\sim$0.5 can be reproduced by mixing the main $(d_{3/2},1p_{1/2}^{-1})$ longitudinal transition providing a $1+1.0P_2(x)$ correlation pattern with a weak $(d_{3/2},1p_{1/2}^{-1})$ transverse component providing a $1-1.0P_2(x)$ or $(s_{1/2},1p_{1/2}^{-1})$ transition which is isotropic. The case of n_3 is more complicated. Configurations of $(s_{1/2},1p_{3/2}^{-1})$, $(d_{5/2},1p_{3/2}^{-1})$, and $(d_{3/2},1p_{3/2}^{-1})$ are assigned for the n_3 transition. The observed b_2 value $\sim$0.5 for n_3 can be reproduced by mixing the main $(d_{5/2},1p_{3/2}^{-1})$ longitudinal transition providing a $1+0.8P_2(x)$ correlation pattern with weak transitions similar to those of n_0.

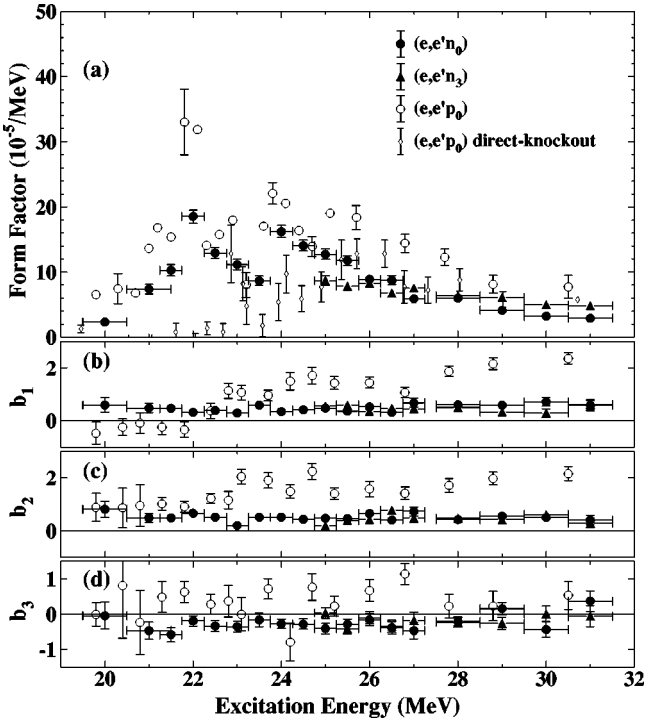

FIG. 5. Comparison of the form factor and angular correlation coefficients b_i for the $^{16}\mathrm{O}(e,e'n_0)$ reaction (solid circles) with those for the $^{16}\mathrm{O}(e,e'n_3)$ (solid triangles) and $^{16}\mathrm{O}(e,e'p_0)$ (open circles) [19] reactions. The open diamonds are the extracted contribution of the direct-knockout process for $(e,e'p_0)$ [19].

The peak at 24 MeV has been historically assigned to result mainly from the $(d_{3/2},1p_{3/2}^{-1})$ configuration using the shell model approach [29]. But from the analysis of $^{11}\mathrm{B}(\vec{p},\gamma_0)^{12}\mathrm{C}$ [30], it has been stated that the main configuration is $(d_{5/2},1p_{3/2}^{-1})$ and the spin-flip $(d_{3/2},1p_{3/2}^{-1})$ component is small. The shift of the peaks in the present angular correlations, described before, is well reproduced by the longitudinal-transverse term, which indicates that the spin-flip component is not dominant for $^{16}\mathrm{O}(e,e'n_3)$, either.

The parameter b_3 indicates interference between $E1$ and $E2$ resonances. The nonzero b_3 value represents the existence of the $E2$ strength. The b_3 value for n_0 remains almost constant up to near 28 MeV, which suggests that the $E2$ strength is broadly distributed. This is consistent with the $E2$ strength obtained by the $^{15}\mathrm{N}(\vec{p},\gamma_0)\mathrm{O}^{16}$ reaction [6,7].

IV. DISCUSSION

A. Comparison of the angular correlation with the theory

In a previous paper [15], we compared the angular correlation for the $^{12}\mathrm{C}(e,e'n_0)$ reaction in the giant resonance region with the predictions by Cavinato *et al.* [25]. In their calculation, the $(e,e'n_0)$ angular correlation shows a behavior that is nearly symmetric about $\theta_n = 90°$. On the other hand, the $(e,e'p_0)$ displays a strong forward-backward asymmetry as a result of interference between the 1^- and 0^+

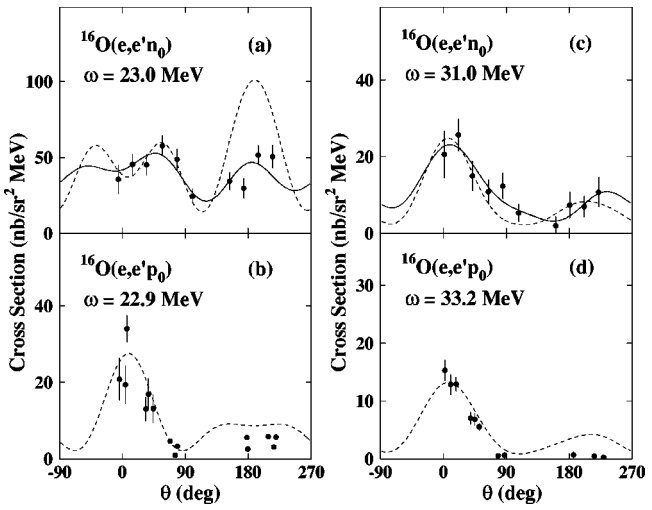

FIG. 6. Comparison of the experimental angular correlation with calculations. The solid circles in (a) and (c) are the present $(e,e'n_0)$ data and those in (b) and (d) are $(e,e'p_0)$ data [19]. The solid lines in (a) and (c) are the same as in Fig. 3. The dashed lines are the predictions by a self-consistent RPA calculation with a SK3 interaction [8]. The calculations in (a) and (b) are done at $\omega = 21$ MeV and those in (c) and (d) are done at $\omega = 30$ MeV. Scaling factors 0.5, 0.1, 3.0, and 1.3 have been applied for (a), (b), (c), and (d), respectively.

modes, where the latter is calculated to be strongly excited in $(e,e'p_0)$. However, the predictions fail to reproduce the experimental angular correlations for both $(e,e'n_0)$ and $(e,e'p_0)$; predicting the opposite pattern to that observed.

Similarly Cavinato *et al.* have calculated the ^{16}O$(e,e'n_0)$ and ^{16}O$(e,e'p_0)$ angular correlations in a self-consistent RPA model with a SK3 interaction for similar kinematical conditions to the present experiment [8]. They show a difference between the $(e,e'n_0)$ and $(e,e'p_0)$ angular correlations depending on the isospin quantum number of the GQR. Specifically the $(e,e'p_0)$ and $(e,e'n_0)$ angular correlations are quite different at $\omega = 21$ MeV due to interference between the IV-GDR and IS-GQR, while they are similar at $\omega = 30$ MeV because of interference between the same IV-GDR and IV-GQR.

Figure 6 compares the measured angular correlations with the calculations. The dashed and solid lines in the figure are the calculations and Legendre polynomial fits, respectively. The single-particle energy predicted by the HF-SK3 calculation is about 2 MeV lower than the experimental value [9], so the calculations are compared with the experimental results at an energy about 2 MeV higher. In Figs. 6(a) and 6(b), a strong backward peak in $(e,e'n_0)$ and a strong forward peak in $(e,e'p_0)$ were predicted due to interference between the GDR and IS-GQR. In Figs. 6(a) and 6(b) the calculated values have been scaled down by factors 0.5 and 0.1, respectively. The forward shape is well reproduced in the $(e,e'n_0)$ reaction in Fig. 6(a). The unique correlation with three peaks of the theoretical curve may be the effect of the interference term $P_3(x)$ in Eq. (3.6). This peak shape means that the sign of the $P_3(x)$ term—namely, the sign of the b_3 parameter—is negative, which is consistent with our result as shown in Fig. 5. However, the present result does not have a strong backward peak which has been theoretically predicted.

One of the reasons of the disagreement for the $(e,e'n_0)$ reaction might be excessively strong excitation of the GQR in the calculations. This RPA calculation does not take into account the spreading width of the IS-GQR, resulting from more complicated particle-hole configurations than $1p$-$1h$. Some RPA calculations including $2p$-$2h$ [31,32] have shown broadening of the IS-GQR in ^{16}O. Another possibility might be the effect that the α-decay channel is not included in this calculation. According to Faessler *et al.* [33], decay by alpha emission might be favored because of the large overlap between the IS-GQR in ^{16}O and the ^{12}C$+\alpha$ channel. The fraction of decay by proton emission has been experimentally found to be very small from the ^{16}O$(\alpha,\alpha'p)$ measurement [3]. And recent theoretical calculations have shown that the ^{12}C$+\alpha$ decay channel even modifies the structure of the GQR for the $(e,e'p_0)$ and $(e,e'p_3)$ reactions [34]. These suggest the same situation for neutron decay. On the other hand, the asymmetry of the p_0 channel in Fig. 6(b) seems to be reproduced well, but it changes drastically around 22 MeV as mentioned in the next section. This change in the $(e,e'p_0)$ angular correlation makes it difficult to compare with the theory.

In Figs. 6(c) and 6(d), the calculations for $(e,e'n_0)$ and $(e,e'p_0)$ are scaled up by 3.0 and 1.3, respectively. They predict a similar correlation for $(e,e'n_0)$ and $(e,e'p_0)$ due to interference between the GDR and IV-GQR. The experimental forward-backward asymmetry of $(e,e'n_0)$ is reproduced well. On the other hand, the correlation for $(e,e'p_0)$ is in agreement at forward angles but is poor at backward angles. The momentum transfer for the $(e,e'p_0)$ data is higher than that in the calculation. This disagreement might be due to the direct-knockout process as discussed in the following section. The predicted character of the forward-backward asymmetry, which depends on the isospin quantum number of the GQR, was not clearly observed through $E1$-$E2$ interference which was seen in the present angular correlations.

B. Comparison with the ^{16}O$(e,e'p_0)$ reaction

The form factor and b_1, b_2, and b_3 parameters for the ^{16}O$(e,e'p_0)$ reaction [19] are shown together with $(e,e'n_0)$ in Fig. 5. The $(e,e'p_0)$ form factor shows two peaks in the GDR, which is dominant even at the higher momentum transfer of $q \sim 0.53$ fm^{-1} than that in the present experiment. Above 22 MeV the peak at the momentum transfer direction in the $(e,e'p_0)$ reaction has been interpreted as being due to the direct-knockout process [19]. Its estimated contribution is shown by open diamonds in Fig. 5(a). The large increase in that process above 22 MeV has been attributed to suppression at lower energies as a result of α clustering [19]. On the other hand, the present parameters b_1 and b_2, which lead to forward peaking, are small compared to p_0. This is consistent with the fact that the direct-knockout process for neutrons is much smaller than for protons in the present scattering conditions where longitudinal (charge) transitions are dominant.

Below 22 MeV the b_2 values are similar but the b_1 and b_3 values are of opposite sign, with nearly the same amplitudes for both reactions. Although the $(e,e'p_0)$ data have poor statistics, the trend is supported by good-quality data from Mainz [20]. This might be explained by interference between the GDR and IS-GQR, which was pointed out by Saruis [10] as follows.

The longitudinal transition amplitude for a decay particle with isospin τ_{3i} is related to that of the resonance with isospin T [10]:

$$L_J^c(\tau_{3i}) = \sum_{T=0,1} \left\langle \frac{1}{2} \quad \frac{1}{2} \quad \tau_{3i} \quad -\tau_{3i} \quad | \quad T \quad 0 \right\rangle L_J^c(T). \tag{4.1}$$

Here, c represents a reaction channel and J is the total angular momentum of a resonance. The structure function of the longitudinal transition W_{L} is proportional to the product of $L_J^c(\tau_{3i})^* L_{J'}^c(\tau_{3i}) + L_J^c(\tau_{3i}) L_{J'}^c(\tau_{3i})^*$ and the Legendre function $P_l(x)$. The observed opposite signs for the b_1 and b_3 terms for $(e,e'p_0)$ and $(e,e'n_0)$ as a result of interference between the IV-GDR and IS-GQR can be easily derived. In a macroscopic view, this effect reflects the out-of-phase vibrations of the proton and neutron groups for the IV-GDR, while these are in phase for the IS-GQR. The $E0$ excitation which can also contribute to the b_1 parameter in ^{16}O has not yet been experimentally confirmed in the present energy region.

C. Comparison between the ^{16}O$(e,e'n_3)$ and ^{12}C$(e,e'n_0)$ reactions

A comparison between the $^{16}\mathrm{O}(e,e'n_3)$ and $^{12}\mathrm{C}(e,e'n_0)$ reactions is interesting as they have the same particle-hole configuration: namely, a $1p_{3/2}$ neutron hole. The fit parameters obtained from the measurements under the same experimental condition are compared in Fig. 7. The GDR in ^{12}C has two peaks at 22.5 and 25.5 MeV similar to ^{16}O. The form factor for $^{16}\mathrm{O}(e,e'n_3)$ is a little smaller than that for $^{12}\mathrm{C}(e,e'n_0)$ in the overlapping region of the excitation energy. The parameters b_i for both reactions agree well in both value and trend. The b_2 values for $^{16}\mathrm{O}(e,e'p_3)$ and $^{12}\mathrm{C}(e,e'p_0)$ [35] are very similar to the present value around 26 MeV.

The $^{12}\mathrm{C}(e,e'n_0)$ reaction has a strong forward peak in the GDR [15,17], and the possibility of an $E0$ resonance has been shown by multipole expansion analysis [17]. The $^{12}\mathrm{C}(e,e'p_0)$ experiment [36] has a localized monopole strength near 20.3 MeV resulting from a large negative b_1 value. A recent $^{12}\mathrm{C}(\alpha,\alpha')$ experiment [37] has obtained an $E0$ peak near the same energy. The large b_1 value for $^{12}\mathrm{C}(e,e'n_0)$, which may reflect this $E0$ state, reduces as the excitation energy goes up and connects smoothly to the b_1 data of $^{16}\mathrm{O}(e,e'n_3)$. On the other hand, the b_1 value for $^{16}\mathrm{O}(e,e'n_0)$ shown in Fig. 5 looks smooth at lower energies, which suggests a different interference from $^{12}\mathrm{C}(e,e'n_0)$. The b_3 parameters for $^{16}\mathrm{O}(e,e'n_3)$ and $^{12}\mathrm{C}(e,e'n_0)$ are in agreement and seem to be negative. This may imply a contribution of $E2$ strength in both reactions.

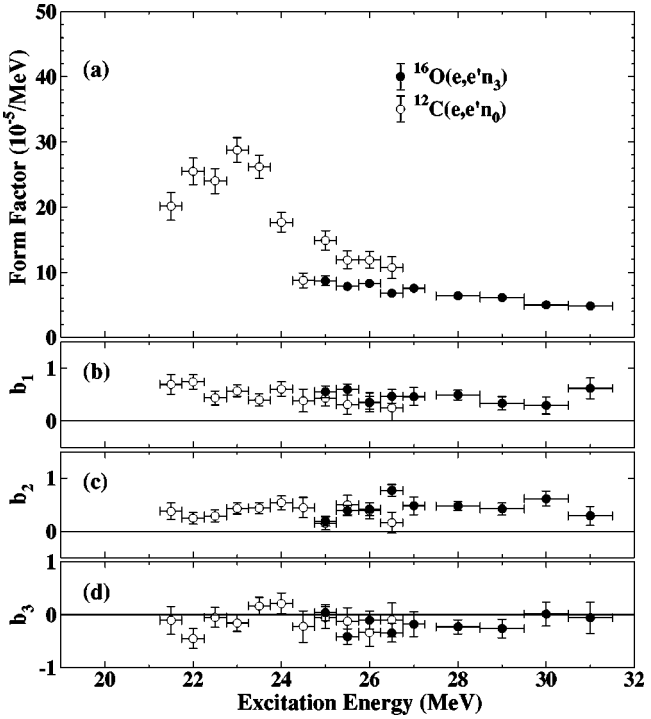

FIG. 7. Comparison of the form factor and angular correlation coefficients b_i for the $^{16}\mathrm{O}(e,e'n_3)$ reaction with those for the $^{12}\mathrm{C}(e,e'n_0)$ reaction under the same experimental conditions.

D. Comparison with the photoneutron reaction

The cross section for the photoneutron reaction [24,38] has been transformed into the form factor by the usual method [14], which assumes that the photoneutron cross section is completely an $E1$ transition. They are compared with the present data in Figs. 8(a) and 9. Both $^{16}\mathrm{O}(e,e'n_0)$ and $^{16}\mathrm{O}(\gamma,n_0)$ form factors agree well not only in strength but also regarding the GDR fine structure. This implies that the $(e,e'n_0)$ strength is almost exhausted by the GDR. On the other hand, the form factor for $(e,e'n_3)$ is about twice as large as that for $(\gamma,n\gamma_3')$ in the overlap region. Even if the $(\gamma,n\gamma_{1,2}')$ and $(\gamma,n\gamma_4')$ form factors add to $(\gamma,n\gamma_3')$, the form factor for electron scattering is still a little larger than that for the photoreaction.

The angular correlation parameters a_1, a_2, and a_3 used in the photoreaction analysis can be related to the parameters b_1, b_2, and b_3 for coincidence electron scattering [27]. The a_2 parameter can be transformed directly to b_2 if only $E1$ is excited. The transformations for a_1 and a_3 to b_1 and b_3 can be achieved through interference between $E1$ and $E2$ as $E0$ does not contribute in the photoreaction. Using Siegert's theorem [28], the transverse transition matrix element was transformed into the longitudinal one at the same momentum transfer. The momentum transfer dependences $j_1(qR)$ and $j_2(qR)$ (R is the nuclear radius) were assumed for $E1$ and $E2$ form factors from the Goldhaber-Teller [39] and Tassie [40] models, respectively. Using them, the transition matrix element was transformed into one at $q=0.33$ fm^{-1} from the photon point. Consequently, for the present $(e,e'n)$ experi-

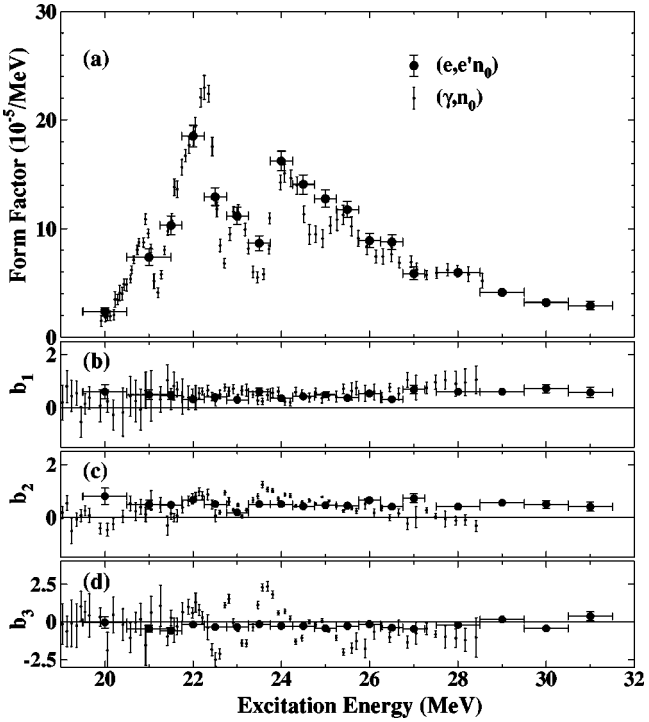

FIG. 8. Comparison of the form factor and angular correlation coefficients b_i for the ^{16}O$(e,e'n_0)$ reaction with those for the ^{16}O(γ,n_0) reaction [38]. The (γ,n_0) data have been extrapolated to the present q value by the method described in the text.

ment, the following relation was obtained for an excitation energy ω and a momentum transfer q:

$$b_1=\frac{4}{3}\frac{q}{\omega}a_1, \tag{4.2}$$

$$b_2=-2a_2, \tag{4.3}$$

$$b_3=-2\frac{q}{\omega}a_3. \tag{4.4}$$

The comparison of the parameters between ^{16}O$(e,e'n_0)$ and ^{16}O(γ,n_0) is shown in Figs. 8(b)–8(d). The b_2 values for both reactions agree fairly well. This implies a similarity for the $E1$ excitation and the decay mechanism for both reactions as indicated in the form factors. One of the interference parameters b_1 is in good agreement for both reactions, but for b_3 the fluctuation in (γ,n_0) was not observed in $(e,e'n_0)$. A smooth b_3 behavior is observed for the ^{16}O$(e,e'p_0)$ [19] and ^{15}N$(\vec{p},\gamma_0)$ [41] reactions, which supports the present data.

V. SUMMARY

The angular correlations for the ^{16}O$(e,e'n_0)$ and ^{16}O$(e,e'n_3)$ reactions were measured in the excitation energy range of 20–31 MeV at a momentum transfer of 0.33 fm^{-1}. These angular correlations were fitted with a series of Legendre polynomials in order to compare with other reactions. These angular correlations, which are very similar, indicate the dominance of the GDR. From an analysis of the b_2 values for n_0 and n_3 transitions, their main configurations are assigned to be $(d_{3/2},1p_{1/2}^{-1})$ and $(d_{5/2},1p_{3/2}^{-1})$, respectively. The interference parameters b_1 and b_3 suggest the presence of $E2$ strength up to 28 MeV. A predicted backward-peaked angular correlation in the neutron decay due to interference between the $T=1$ GDR and $T=0$ GQR was not observed. The isoscalar nature of the $E2$ resonance for the ^{16}O$(e,e'n_0)$ and ^{16}O$(e,e'p_0)$ reactions below about 22 MeV is suggested by the opposite signs of the parameters b_1 and b_3. Above about 22 MeV, large positive values of b_1 and b_2 in $(e,e'p_0)$ compared with small ones in $(e,e'n_0)$ reflect a contribution due to the direct-knockout process in $(e,e'p_0)$. The ^{16}O$(e,e'n_3)$ and ^{12}C$(e,e'n_0)$ angular correlations were confirmed to be similar as expected from the similarity of their particle-hole configurations. Good agreement including the fine structure for both ^{16}O$(e,e'n_0)$ and ^{16}O(γ,n_0) form factors, confirmed GDR dominance in this energy region. The b_1 and b_2 parameters for both reactions agree well, but the behavior of b_3 is quite different.

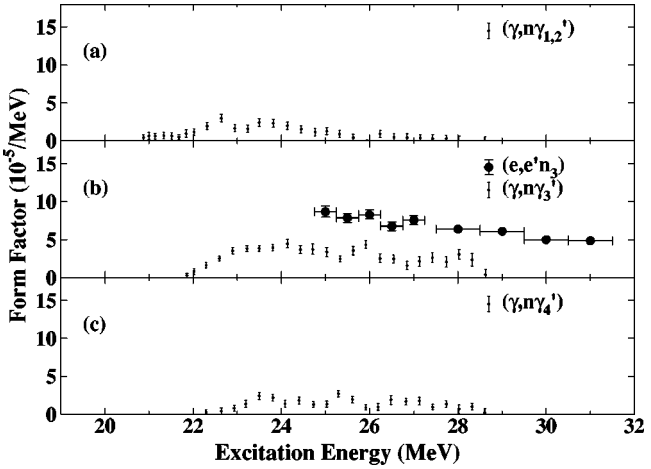

FIG. 9. Comparison of the present ^{16}O$(e,e'n_3)$ strength with (a) ^{16}O$(\gamma,n\gamma'_{1,2})$, (b) $(\gamma,n\gamma'_3)$, and (c) $(\gamma,n\gamma'_4)$ reactions [24]. The extrapolation for the photoreaction data is the same as in Fig. 8.

ACKNOWLEDGMENTS

We wish to thank Professor R. Neuhausen for making available the result of Mainz data in advance of publication and comments. We are grateful to Professor M.N. Thompson for a careful reading of the manuscript and helpful discussions. We would like to thank the linac crew of the Laboratory of Nuclear Science for providing the quality beam.

[1] K. T. Knöpfle, G. J. Wagner, H. Breuer, M. Rogge, and C. Mayer-Böricke, Phys. Rev. Lett. **35**, 779 (1975).
[2] M. N. Harakeh, A. R. Arends, M. J. A. de Voigt, A. G. Drentje, S. Y. van der Werf, and A. van der Woude, Nucl. Phys. **A265**, 189 (1976).
[3] K. T. Knöpfle, G. J. Wagner, P. Paul, H. Breuer, C. Mayer-Böricke, M. Rogge, and P. Turek, Phys. Lett. **74B**, 191 (1978).
[4] J. P. Fritsch, H. J. Emrich, A. Grasmück, R. Neuhausen, S. Schardt, N. Zimmermann, J. R. Calarco, and M. Potokar, Phys. Rev. Lett. **68**, 1667 (1992).
[5] T. W. Phillips and R. G. Johnson, Phys. Rev. C **20**, 1689 (1979).
[6] S. S. Hanna, H. F. Glavish, R. Avida, J. R. Calarco, E. Kuhlmann, and R. LaCanna, Phys. Rev. Lett. **32**, 114 (1974).
[7] S. W. Wissink, S. S. Hanna, D. G. Mavis, and T. R. Wang, Phys. Rev. C **37**, 2289 (1988).
[8] M. Cavinato, M. Marangoni, and A. M. Saruis, Phys. Lett. **163B**, 49 (1985).
[9] M. Cavinato, M. Marangoni, and A. M. Saruis, Phys. Rev. C **37**, 1823 (1988).
[10] A. M. Saruis, Phys. Rep. **235**, 57 (1993).
[11] G. O. Bolme, L. S. Cardman, R. Doerfler, L. J. Koester, Jr., B. L. Miller, C. N. Papanicolas, H. Rothhaas, and S. E. Williamson, Phys. Rev. Lett. **61**, 1081 (1988).
[12] R. A. Miskimen *et al.* Phys. Lett. B **236**, 251 (1990).
[13] R. A. Miskimen *et al.*, Phys. Rev. C **43**, 1677 (1991).
[14] C. Takakuwa, T. Saito, S. Suzuki, K. Takahisa, T. Tohei, T. Nakagawa, and K. Abe, Phys. Rev. C **50**, 845 (1994).
[15] T. Saito, S. Suzuki, K. Takahisa, C. Takakuwa, M. Oikawa, T. Tohei, T. Nakagawa, and K. Abe, Phys. Rev. Lett. **78**, 1018 (1997).
[16] S. Suzuki, T. Saito, K. Takahisa, C. Takakuwa, T. Nakagawa, T. Tohei, and K. Abe, Phys. Rev. C **60**, 034309 (1999).
[17] M. Oikawa, T. Saito, K. Takahisa, Y. Suga, K. Kino, T. Nakagawa, T. Tohei, K. Abe, and H. Ueno, Phys. Rev. Lett. **84**, 2338 (2000).
[18] S. Strauch, P. von Neumann-Cosel, C. Rangacharyulu, A. Richter, G. Schrieder, K. Schweda, and J. Wambach, Phys. Rev. Lett. **85**, 2913 (2000).
[19] V. F. Dmitriev, D. M. Nikolenko, S. G. Popov, I. A. Rachek, D. K. Toporkov, E. P. Tsentalovich, B. B. Woitsekhowski, and V. G. Zelevinsky, Nucl. Phys. **A464**, 237 (1987).
[20] N. Zimmermann, Ph. D. thesis, University of Mainz, 1988; R. Neuhausen (private communication).
[21] T. Tamae *et al.*, Nucl. Instrum. Methods Phys. Res. A **264**, 173 (1988).
[22] R. R. Doering, D. M. Patterson, and A. Galonsky, Phys. Rev. C **12**, 378 (1975).
[23] S. Suzuki, T. Saito, K. Takahisa, C. Takakuwa, T. Tohei, T. Nakagawa, Y. Kobayashi, and K. Abe, Nucl. Instrum. Methods Phys. Res. A **314**, 547 (1992).
[24] J. T. Caldwell, S. C. Fultz, and R. L. Bramblett, Phys. Rev. Lett. **19**, 447 (1967).
[25] M. Cavinato, D. Drechsel, E. Fein, M. Marangoni, and A. M. Saruis, Nucl. Phys. **A444**, 13 (1985).
[26] A. Hotta, K. Itoh, and T. Saito, Phys. Rev. Lett. **33**, 790 (1974).
[27] W. E. Kleppinger and J. D. Walecka, Ann. Phys. (N.Y.) **146**, 349 (1983).
[28] A. J. F. Siegert, Phys. Rev. **52**, 787 (1937).
[29] G. E. Brown, L. Castillejo, and J. A. Evans, Nucl. Phys. **22**, 1 (1961).
[30] R. G. Allas, S. S. Hanna, L. Meyer-Schützmeister, and R. E. Segel, Nucl. Phys. **58**, 122 (1964).
[31] T. Hoshino and A. Arima, Phys. Rev. Lett. **37**, 266 (1976).
[32] J. S. Dehesa, S. Krewald, J. Speth, and A. Faessler, Phys. Rev. C **15**, 1858 (1977).
[33] A. Faessler, D. J. Millener, P. Paul, and D. Strottman, Nucl. Phys. **A330**, 333 (1979).
[34] M. Buballa, A. Gattone, R. de Haro, R. Jessenberger, and S. Krewald, Nucl. Phys. **A517**, 61 (1990).
[35] J. R. Calarco, Nucl. Phys. **A569**, 363c (1994).
[36] J. R. Calarco, J. Arruda-Neto, K. A. Griffioen, S. S. Hanna, D. H. H. Hoffmann, B. Neyer, R. E. Rand, K. Wienhard, and M. R. Yearian, Phys. Lett. **146B**, 179 (1984).
[37] D. H. Youngblood, Y.-W. Lui, and H. L. Clark, Phys. Rev. C **57**, 2748 (1998).
[38] J. W. Jury, J. S. Hewitt, and K. G. McNeill, Can. J. Phys. **48**, 1635 (1970).
[39] M. Goldhaber and E. Teller, Phys. Rev. **74**, 1046 (1948).
[40] L. J. Tassie, Aust. J. Phys. **9**, 407 (1956).
[41] W. J. O'Connell and S. S. Hanna, Phys. Rev. C **17**, 892 (1978).